

# **Asymmetric and Anharmonic Electrode Kinetics: Evaluation of a Model for Electron Transfer with Concerted Rupture of Weak, Inner Shell Interactions**

Nathan S. Lawrence,<sup>1</sup> Bernd Schöllhorn,<sup>2</sup> Jay D. Wadhawan<sup>\*1</sup>

<sup>1</sup>*Department of Chemical Engineering, The University of Hull,  
Cottingham Road, Kingston-upon-Hull HU6 7RX, United Kingdom.*

<sup>2</sup>*Université de Paris - Laboratoire d'Electrochimie Moléculaire,  
CNRS, F-75006, Paris, France.*

This is the peer reviewed version of the following article: N. S. Lawrence, B. Schöllhorn, J. D. Wadhawan, *ChemistrySelect* 2021, 6, 13331, which has been published in final form at <https://doi.org/10.1002/slct.202103526>. This article may be used for non-commercial purposes in accordance with Wiley Terms and Conditions for Use of Self-Archived Versions. This article may not be enhanced, enriched or otherwise transformed into a derivative work, without express permission from Wiley or by statutory rights under applicable legislation. Copyright notices must not be removed, obscured or modified. The article must be linked to Wiley's version of record on Wiley Online Library and any embedding, framing or otherwise making available the article or pages thereof by third parties from platforms, services and websites other than Wiley Online Library must be prohibited.

*Dedicated to the memory of the late, and inspirational, Professor Jean-Michel Savéant.*

To be communicated to *ChemistrySelect*

\*Author to whom all correspondence should be addressed.

E.mail: [j.wadhawan@hull.ac.uk](mailto:j.wadhawan@hull.ac.uk)

## **Abstract**

A surface-integrated form of the widely used (anharmonic) Lennard-Jones 12-6 interaction potential, the Lennard-Jones 9-3 potential, is used to develop a quadratic activation/driving force relationship that gives rise to asymmetric Tafel plots for electron transfer occurring with simultaneous interaction rupture. The Tafel plots are shown to exhibit linearity over a wide potential range, depending on the ratio of the Gibbs interaction well to the solvent reorganisation free energy. The fit of the model to experimental data for a ferrocene-based self-assembled monolayer (SAM) bathed by aqueous perchloric acid suggests ion pairing between ferricenium and perchlorate ions. This crude and primitive model readily enables experimentalists to obtain a parametric understanding of the physicochemical dynamics underpinning interaction rupture in concert with electron transfer, which may empower routes to improve the efficiency of a plethora of topical electrochemical technologies.

The present demand to deploy green and sustainable technologies for a whole host of industrial sectors has encouraged process electrification, which, in turn has empowered a growth in electrochemical technologies for, *inter alia*, energy conversion and storage, chemical manufacture, and water treatment.<sup>[1]</sup> The efficiency of many of these technologies is dependent on the kinetics of the electrode reactions. Whilst activation/driving force relationships at electrodes (Tafel plots) are typically non-linear at metallic electrodes, they can be *asymmetric* in some cases, resulting from unequal force constants for the harmonic vibrational modes of the oxidised and reduced species.<sup>[2],[3]</sup> In two documented examples, *viz.*, silver metal deposition<sup>[4]</sup> and hydrogen evolution,<sup>[5]</sup> asymmetric Tafel plots have been recognised as being derived from *anharmonic potential energy profiles*.

Although *mechanical anharmonicity* is widely appreciated as being important for electrode reactions in which bond cleavage occurs in concert with electron transfer,<sup>[6],[7]</sup> “local mode anharmonicity”<sup>[8]</sup> is also important during a variety of inner-sphere electron transfer processes, such as ligand substitution,<sup>[9]</sup> and atom transfers in chemistry<sup>[10]</sup> and biology,<sup>[11]</sup> where its effect, even under the simplified treatment of high frequency bond stretches in the ground state,<sup>[4]</sup> is to alter the curvature of the activation/driving force relationship, compared with the harmonic case:<sup>[10],[12]</sup> it increases the value of the transition probability due to reducing the barrier height and width for electron tunnelling.<sup>[13]</sup> For electrochemical electron transfer reactions, such local mode anharmonicity results in asymmetric Tafel plots,<sup>[4],[5],[12]</sup> which can be linear for over 1 V at some metals.<sup>[5]</sup> In contrast, for bimolecular, homogeneous electron transfer processes, the two quantum mode displacements (symmetric stretch on one reacting species, and compression on the other) have opposing effects which essentially cancel the observation of anharmonicity in the normal region,<sup>[12]</sup> as observed for electron self-exchange kinetics associated with naphthalene/naphthalene radical anion ion pairs.<sup>[14],[15]</sup>

Anharmonic electron transfer requires the assumption of an *empirical* potential energy profile<sup>[16]</sup> – whether it is based on a simple analytical expression, such as the Morse curve<sup>[17]</sup> (or the mathematically related<sup>[18]</sup> Lennard-Jones 12-6 intermolecular potential<sup>[19]</sup>), or one derived from quantum calculations.<sup>[16]</sup> The former have been more popular, owing to their quadratic nature,<sup>[20]</sup> despite simple and computationally facile, parametric algorithms having been developed to characterise anharmonic effects “beyond single-mode quadratic forms.”<sup>[21]</sup> The famous quadratic model developed by Savéant<sup>[6],[7]</sup> assumes a low frequency vibration for the solvent polarisation (continuum theory), which is treated classically, with a single, significantly anharmonic (Morse curve), high frequency, local mode. This model has been applied most to experimental data, since it does not require computational simulation of the energy barrier with driving force.<sup>[21]</sup>

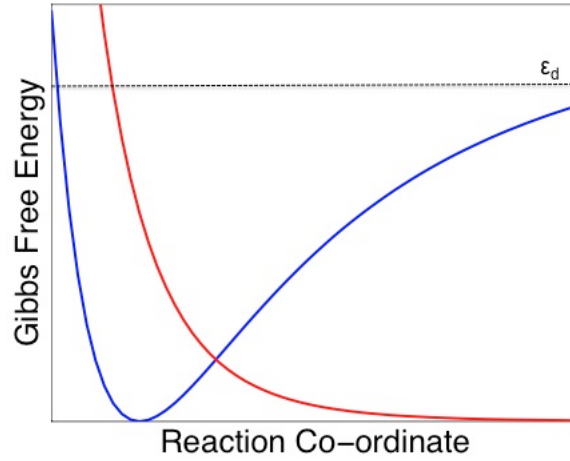
Although highly successful and popular, one of the drawbacks of Savéant’s model is that it does not account for asymmetric Tafel plots.<sup>[23]</sup> Accordingly, in this contribution, we investigate a quadratic model that allows for simultaneous electron transfer with weak bond

rupture, where the occurrence of *electrical anharmonic* effects, such as those which may be induced by the electric field at the electrode | electrolyte interface, may occur. Indeed, for these systems, both a first-order (change in static charge distribution through redox species/electrode interaction) and a second-order (field-induced molecular electronic polarisation) Stark effect might be anticipated.<sup>[24]</sup>

The approach we take is primitive: over the last few decades, very fine computational quantum chemical methods have been popularised,<sup>[25-29]</sup> but these developments are difficult for non-specialists to apply directly to experimental data (which may include battery performance curves) than analytical expressions. Accordingly, our mathematically convenient approach, albeit crude and approximate, is pragmatic and accessible through being relatively non-cumbersome in its deployment. For this, we make an oversimplification: we assume a Lennard-Jones 9-3 model (Figure 1) to describe the potential energy curve for the reactants. Although this may appear physically unrealistic, this interaction derives from a surface-integrated Lennard-Jones 12-6 potential.<sup>[30],[31]</sup> The latter is extremely popular in molecular simulations,<sup>[32]</sup> and can be mathematically transformed to yield to the Morse potential.<sup>[18]</sup> Indeed, the use of the 12-6 potential yields exactly the same (symmetric) activation/driving force relationship as that of Savéant's Morse curve model. The 9-3 interaction has found prior use in studying the effects of water-wall interactions in nano-confined water,<sup>[33],[34]</sup> and in describing water in simple electrical double layers.<sup>[35]</sup> The model is equivalent to changing the exponent of the dissociation state in Savéant's model, to one that is different to the corresponding repulsive exponent in the Morse potential for the bound state. We apply this model to the case of an electron transfer that is thought to occur in concert with the breaking of an ion pair. Both Savéant<sup>[36],[37]</sup> and Schmickler *et al.*<sup>[38]</sup> have described this process using Morse curves, even though this might not be the most appropriate model for ion pairing. There is limited justification for our approach since ion pairing interactions have been described as the summation of a 12-6 potential with an R<sup>-1</sup> Coulombic energy,<sup>[39]</sup> although this moves to an R<sup>-3</sup> term,<sup>[40]</sup> if the ion pairing interaction is considered as occurring over larger distances, so that it is to be dominated by dipole-dipole type interactions (which vary as R<sup>-6</sup>, and which integrate over a surface to afford an R<sup>-3</sup> term).<sup>[30],[31]</sup>

For metallic electrodes, where the driving force for an heterogeneous electron transfer is  $-\Delta G^0 = -[(E_F - E) + q_0(U - U^0)]$ , where E is the electronic energy in the metal, with E<sub>F</sub> being the Fermi level; q<sub>0</sub> is the electronic charge; and (U - U<sup>0</sup>) is the applied overpotential, the continuous electronic energy spectrum in the electrode causes the rate constant (k<sub>t/b</sub>) for heterogeneous electron transfer to follow the form given in equation (1),<sup>[41-44]</sup>

**Figure 1**



*Gibbs energy profile (along the nuclear co-ordinate) for the Lennard-Jones 9-3 interaction considered in this work, for an isogonic electron transfer pathway. The blue and red diabatic curves correspond to reactants (R) and products (P), respectively, and are of the form*

$$G_R = G_R^{eqm} + \lambda_s X^2 + \varepsilon_d \left\{ 1 + \frac{3\sqrt{3}}{2} Y(Y^2 - 1) \right\} \text{ and } G_P = G_P^{eqm} + \lambda_s (1 - X)^2 + \frac{3\sqrt{3}}{2} \varepsilon_d Y^3$$

*where  $X$  is the solvent index:  $X = z_R - z_{dummy}$  and  $z_P = z_R - 1$  ( $z_i$  is the charge on  $i = R$  or  $P$ );  $G_i^{eqm}$  is the Gibbs energy of state  $i$*

*at equilibrium, such that the Gibbs energy change for the electron transfer reaction is  $\Delta G^0 = G_P^{eqm} - G_R^{eqm}$*

*; the reduced nuclear co-ordinate,  $Y$ , is given as  $Y = \left( \frac{\sigma}{R} \right)^3$ , where  $\sigma$  is the hard sphere diameter of the*

*reactants, and  $R = y + 3^{1/6} \sigma$  defines the distance between the reactant and the electrode, relative to the free energy minimum. Note that the transition state occurs when  $G_R = G_P$ .*

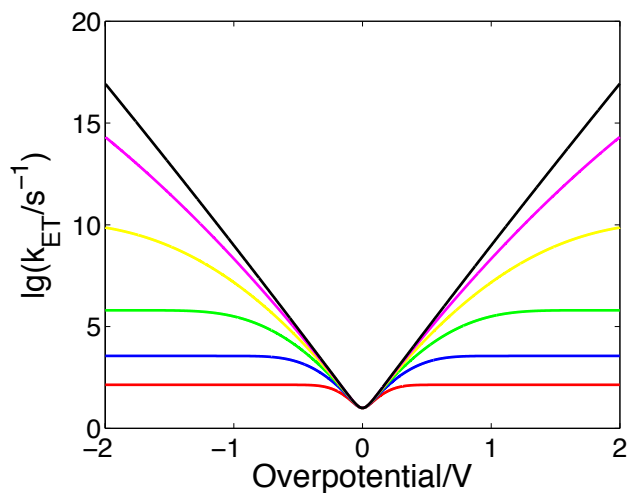
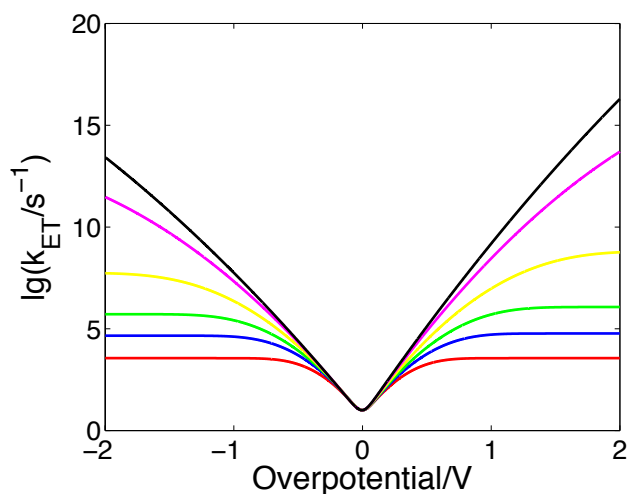
$$k_{f/b} = K \int_{-\infty}^{\infty} \frac{\exp\left(-\frac{\Delta G_{f/b}^\ddagger}{k_B T}\right)}{1 + \exp\left[\pm \frac{(E - E_F)}{k_B T}\right]} dE \quad (1)$$

in which  $k_B T$  is the thermal energy of the system (0.0257 eV at 298 K);  $K$  is a constant assumed to be independent of the electronic energy, and is proportional to the electronic coupling matrix element for the metal electrode and the reacting redox species, and the density of states (the number of electronic states per atom per unit energy) in the electrode at the Fermi energy;  $\Delta G_{f/b}^\ddagger$  is the activation free energy for the forward (f), reductive (+), bond-breaking, or reverse (b) oxidative (-), bond-forming electron transfer reactions. The activation barrier in equation (1) is given in terms of free energy, rather than potential energy, since the transition probability has to account for the uncertainty owing to the thermal population of the vibrational states in the reactants, which yields an entropic contribution to the activation barrier (although this is typically much smaller than the entropic contributions to the solvent reorganisation free energy<sup>[45],[46]</sup>). Thus, if the Gibbs energy wells for reactants and products are assumed to be parabolic (with equal force constants for both oxidised and reduced species), or if the Gibbs barrier follows Savéant's Morse curve model (or, equivalently, the Lennard-Jones 12-6 form),<sup>[6],[7],[23]</sup> the symmetric Tafel plots illustrated in Figure 2a result. However, using a Lennard-Jones 9-3 form, for which the Gibbs activation energies are given in equation (2),

$$\Delta G_f^\ddagger = \frac{\left(\lambda_s + \frac{1}{4}\varepsilon_d\right)\left(\lambda_s + \frac{1}{2}\varepsilon_d\right)^2}{4\left(\lambda_s + \frac{3}{8}\varepsilon_d\right)^2} \left[ 1 + \frac{\Delta G^0}{\left(\lambda_s + \frac{1}{2}\varepsilon_d\right)} \right]^2 \quad (2a)$$

$$\Delta G_b^\ddagger = \frac{\left(\lambda_s + \frac{1}{4}\varepsilon_d\right)\left(\lambda_s + \frac{1}{2}\varepsilon_d\right)^2}{4\left(\lambda_s + \frac{3}{8}\varepsilon_d\right)^2} \left[ \left[ 1 - \frac{\Delta G^0}{\left(\lambda_s + \frac{1}{2}\varepsilon_d\right)} \right]^2 - \Delta G^0 \frac{\frac{1}{16}\varepsilon_d^2}{\left(\lambda_s + \frac{1}{4}\varepsilon_d\right)\left(\lambda_s + \frac{1}{2}\varepsilon_d\right)^2} \right] \quad (2b)$$

where  $\lambda_s$  is the solvent reorganisation free energy and  $\varepsilon_d$  represents the Gibbs energy well corresponding to the weak interaction, asymmetric Tafel plots result (Figure 2b). These expressions for the activation free energy derive from the assumed barrier illustrated in Figure 1, which, following the convention employed by Wentworth *et al.*,<sup>[47]</sup> Savéant,<sup>[6]</sup> and German and Kuznetsov,<sup>[48],[49]</sup> has the reactant free energy given by the Lennard-Jones 9-3 model, with the product free energy surface assumed to be only the repulsive part: the interaction between low-energy orbital electrons and the nucleus is assumed to be insignificantly altered by the presence of an extra electron in the frontier orbitals. Accordingly, the transition state is located as the saddle point between the reactant and product hyperspaces, and can be determined algebraically through Lagrange's method of undetermined multipliers,<sup>[50]</sup> under the assumption that the saddle point is reached with a *small injection of charge, viz.*, an early transition state. It is noteworthy that the expressions

**Figure 2****(a)****(b)**

Variation of the electron transfer rate constant,  $k_{ET} = k_f + k_b$ , with overpotential for a nonadiabatic electron transfer process for reactants immobilised at metallic electrodes, with a standard heterogeneous electron transfer rate constant (viz. that at zero overpotential) of  $5.0 \text{ s}^{-1}$ . (a) Symmetric, harmonic oscillator (or Morse curve model), and (b) asymmetric, anharmonic Lennard-Jones 9-3 model. In (a), the total reorganisation energy,  $\lambda = 0.2$  (red),  $0.5$  (blue),  $1.0$  (green),  $2.0$  (yellow),  $5.0$  (magenta) and  $25 \text{ eV}$  (black). In (b), the solvent reorganisation energy,  $\lambda_s = 0.5 \text{ eV}$ , with various values of the well depth ( $\epsilon_a$ ):  $0.0$  (red),  $0.5$  (blue),  $1.0$  (green),  $2.0$  (yellow),  $5.0$  (magenta) and  $10 \text{ eV}$  (black). Note that by defining the ordinate axis as the summation of the forward and reverse rate constants, the minimum occurs at  $\lg(k_{ET}/\text{s}^{-1}) = 1.0$ .

in equation (2) reduce to the familiar quadratic expression developed by Marcus<sup>[51]</sup> in the limit  $\varepsilon_d \rightarrow 0$ , with the degree of asymmetry controlled by the ratio  $\frac{\varepsilon_d}{\lambda_s}$ : when

$\frac{\varepsilon_d}{\lambda_s} \rightarrow 0$ ,  $\frac{\varepsilon_d^2}{64\left(\lambda_s + \frac{3}{8}\varepsilon_d\right)^2} \rightarrow 0$ , so that symmetric Tafel plots are observed, whilst the maximum

extent of asymmetry, *viz.*  $\frac{\varepsilon_d^2}{64\left(\lambda_s + \frac{3}{8}\varepsilon_d\right)^2} \rightarrow \frac{1}{9}$ , occurs when  $\frac{\varepsilon_d}{\lambda_s} \gg 2.7$ .

The following observations can be made from the Tafel plots in Figure 2. (i) For both cases, at low overpotentials, the plots are linear in both anodic and cathodic regimes, with the rate constants tailing to a maximum at higher overpotentials; (ii) at constant  $\lambda = \lambda_s + \varepsilon_d$ , the anharmonic case *decreases both anodic and cathodic slopes*, compared with the absence of interactions, as the activation barrier is greater in the former case; (iii) the interaction breaking process is slower compared with the interaction forming reaction, as expected; (iv) at constant  $\lambda_s$ , the effect of increasing  $\varepsilon_d$  is to push both forward and reverse processes into the linear Butler-Volmer regime, even at high overpotential, in agreement with the sophisticated previous work on nonadiabatic, anharmonic heterogeneous electron transfer considered by Ulstrup and co-workers,<sup>[5]</sup> and the earlier work by Despić and Bockris.<sup>[4]</sup>

Although Figure 2b shares the qualitative features of the more correct potential for the reactants and products, presented by Ulstrup and co-workers,<sup>[5],[13],[21]</sup> we recognise the weakness of our model though its use of the mathematically convenient, but physically limited, 9-3 Lennard-Jones interaction. We recognise that an extension to Savéant's treatment, where the ratio of the two exponents is not restricted to Savéant's value of two, would, likewise, capture asymmetry in the Tafel plots. Moreover, as mentioned earlier, a more physically realistic interaction might involve a reacting ion pair that has a counter-ion-shielded Debye-type term of the form  $r^{-1}e^{-kr}$ , and either a repulsive Pauli-exclusion based decaying exponential or a Lennard-Jones-type  $r^{-12}$  term per pair; for the products, the attractive shielded ion-ion term would disappear, and there would be a differential exponential repulsive Pauli exclusion term, amongst others. This might be better than the oversimplification incurred through use of the pairwise Lennard-Jones 9-3 interaction employed in this work. Nevertheless, the merit of the model presented is that it shows that there are several interactions that can lead to an asymmetric Tafel plot.

We next consider the application of the model developed in this work to the case for the reduction of dilute, ferrocene-based monolayers on gold in aqueous perchloric acid. In these systems, the partial molar standard entropy of the (oxidised) ferricenium species is slightly larger than that of the (reduced) ferrocene,<sup>[52]</sup> owing to the increased polarisation of water

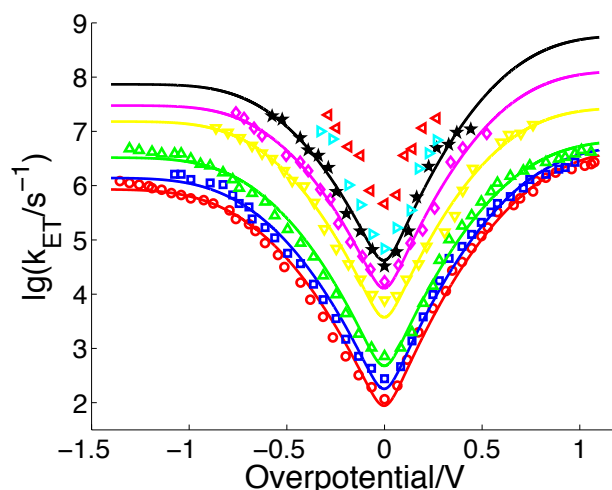
molecules surrounding the reduced form.<sup>[53],[54]</sup> Nevertheless, whilst the standard entropy of the reaction is considered to be small enough to be neglected,<sup>[55]</sup> the experimental discrepancy between the surface monolayer system and that in homogeneous solution is consistent with ion pairing between the monolayer ferricenium ion and the aqueous perchlorate.<sup>[52]</sup> Furthermore, when the ferrocene moiety is not buried inside in the monolayer, the formal potential shifts with perchlorate ion concentration, consistent with a concerted electron/ion transfer process.<sup>[56],[57]</sup> Additionally, a number of authors have suggested that the energy of  $\text{Fc}^+-\text{ClO}_4^-$  ion pairs in self-assembled monolayers can be between 0.2 – 1.5 eV.<sup>[58-60]</sup> Thus, in these systems, reduction of the ferricenium species necessarily breaks the ion pair.

Comparison of the Lennard-Jones 9-3 model with the asymmetric Tafel plots observed experimentally by Chidsey and Robinson,<sup>[61]</sup> for  $\text{FcCO}_2(\text{CH}_2)_n\text{SH}$  ( $5 \leq n \leq 13$ ) self-assembled on a Au(111) surface (ferrocene-SAM), using similar length alkanethiol diluent spacers, in aqueous 1.0 M  $\text{HClO}_4$ , is given in Figure 3. Note that the experimental data were not corrected for double-layer effects, since the model considers the electrolyte ions to be dynamic – being freely available to contact with, adsorb to, and desorb from the electrode surface, precluding the identification of a specific, “fixed” plane of charges, and thereby, giving preference to distance-dependent electron tunnelling.<sup>[62]</sup> Reasonable agreement is observed between the experiment and the model, with  $\epsilon_d = 1.02 \pm 0.20 \text{ eV}$  and  $\lambda_s = 0.27 \pm 0.11 \text{ eV}$  (

$\frac{\epsilon_d}{\lambda_s} = 3.8 \pm 1.7$  indicates that asymmetry is significant).

As anticipated, the rate constant at zero overpotential ( $k_s$ ) holds an exponential dependence on monolayer thickness, with the decay constant  $\sim 1.0 \text{ \AA}^{-1}$ , although  $\lambda = \lambda_s + \epsilon_d = 1.29 \pm 0.31 \text{ eV}$ , is approximately twice as large as that reported using the symmetric, harmonic model.<sup>[61]</sup> The large values of  $\epsilon_d$  are consistent with ion pairing effects. Moreover, the lack of their distance-dependence is suggestive of ionic association, where the perchlorate ion atmosphere around the charged form of the ferrocene is quite localised around the ion. Further, the small<sup>[63]</sup> size of  $\lambda_s$  is consistent with  $\text{Fc}^+-\text{ClO}_4^-$  ion pairs: if the Marcus solvent reorganisation energy equation<sup>[51]</sup> is used as a first approximation,  $\lambda_s = 0.26 \pm 0.06 \text{ eV}$  with the reactant radius being the average of the radii of the ferricenium ion<sup>[52]</sup> (3.8  $\text{\AA}$ ) and solvated perchlorate ion<sup>[64]</sup> (3.1  $\text{\AA}$ ), and with the distance between the metal electrode and the ion pair reactant estimated as 1.25  $\text{\AA}$  per methylene unit. In addition, the activation energy at zero driving force extracted using our model,  $0.19 \pm 0.03 \text{ eV}$ , is consistent with independent experimental results obtained *via* Arrhenius plots for similar systems ( $0.18 \pm 0.01 \text{ eV}$  for  $\text{FcCONH}(\text{CH}_2)_{15}\text{SH}$  with  $\text{HO}(\text{CH}_2)_{16}\text{SH}$  diluent in 1.0 M  $\text{HClO}_4$ ;<sup>[52]</sup>  $0.21 \pm 0.01 \text{ eV}$  for  $\text{FcCO}_2(\text{CH}_2)_n\text{SH}$  with  $\text{CH}_3(\text{CH}_2)_{n-1}\text{SH}$  diluent in 1.0 M  $\text{HClO}_4$  for<sup>[55]</sup>  $5 \leq n \leq 9$ ).

**Figure 3**



Variation of the electron transfer rate constant ( $k_{ET} = k_f + k_b$ ) for ferrocene-based self-assembled monolayers ( $\text{FcCO}_2(\text{CH}_2)_n\text{SH}$  diluted by  $\text{H}(\text{CH}_2)_n\text{SH}$ ) with applied overpotential, on gold electrodes immersed in 1.0 M aqueous perchloric acid. Symbols refer to experimental points; solid lines to those corresponding to the model, using the values in Table 1. Key: red lines and circles:  $n = 13$  ( $U^o = 0.198$  V vs. Ag |  $\text{AgClO}_4$  |  $\text{ClO}_4^-$ ;  $k_s = 43.7 \pm 1.0$  s $^{-1}$ ;  $\lambda_s = 0.24 \pm 0.01$  eV;  $\epsilon_d = 1.24 \pm 0.01$  eV); blue lines and squares:  $n = 12$  ( $U^o = 0.198$  V vs. Ag |  $\text{AgClO}_4$  |  $\text{ClO}_4^-$ ;  $k_s = 90.9 \pm 2.0$  s $^{-1}$ ;  $\lambda_s = 0.27 \pm 0.01$  eV;  $\epsilon_d = 1.10 \pm 0.02$  eV); green lines and triangles:  $n = 11$  ( $U^o = 0.198$  V vs. Ag |  $\text{AgClO}_4$  |  $\text{ClO}_4^-$ ;  $k_s = 240 \pm 1.0$  s $^{-1}$ ;  $\lambda_s = 0.39 \pm 0.01$  eV;  $\epsilon_d = 0.83 \pm 0.02$  eV); yellow lines and inverted triangles:  $n = 10$  ( $U^o = 0.171$  V vs. Ag |  $\text{AgClO}_4$  |  $\text{ClO}_4^-$ ;  $k_s = 18.6 \pm 0.3 \times 10^2$  s $^{-1}$ ;  $\lambda_s = 0.38 \pm 0.02$  eV;  $\epsilon_d = 0.74 \pm 0.03$  eV); magenta lines and diamonds:  $n = 9$  ( $U^o = 0.161$  V vs. Ag |  $\text{AgClO}_4$  |  $\text{ClO}_4^-$ ;  $k_s = 6.49 \pm 0.1 \times 10^3$  s $^{-1}$ ;  $\lambda_s = 0.19 \pm 0.01$  eV;  $\epsilon_d = 1.04 \pm 0.02$  eV); black lines and pentagons:  $n = 8$  ( $U^o = 0.178$  V vs. Ag |  $\text{AgClO}_4$  |  $\text{ClO}_4^-$ ;  $k_s = 20.5 \pm 0.5 \times 10^3$  s $^{-1}$ ;  $\lambda_s = 0.11 \pm 0.01$  eV;  $\epsilon_d = 1.19 \pm 0.04$  eV); cyan triangles:  $n = 7$ ; red triangles:  $n = 5$ . Data fitting given only for  $n > 7$ , owing to the insufficient data available at higher overpotentials for  $n \leq 7$ . Experimental data obtained from Figure 5 in reference [61]; adapted with permission from the American Chemical Society.

In summary, we have presented a “rough and ready”, quadratic, anharmonic model in which concerted electron transfer/interaction breakage takes place, and which afford asymmetric Tafel plots at metallic electrodes. The qualitative features captured by this model agree with those developed earlier by others.<sup>[4],[5]</sup> Application of our primitive model to the case of electron transfer between an electrode and a ferrocene-SAM immersed in perchloric acid has indicated that the size of the interaction between cation and anion is significant. Such interactions might play an important rôle in current electrochemical technologies, such as lithium-ion batteries, where solvent and anion effects have been recently demonstrated to afford asymmetric Tafel plots,<sup>[65],[66]</sup> and which may influence their *in operando* performance characteristics.

### Supporting Information Summary

Details of the computational methods used are outlined in the Supporting Information.

### Conflicts of Interest

The authors declare no competing financial interests.

### Acknowledgements

We thank EPSRC (grant number EP/Go20833/1) and The University of Hull for funding this work. We express sincere gratitude to five anonymous reviewers for their advice, criticisms and sharp reading of this work.

### Keywords

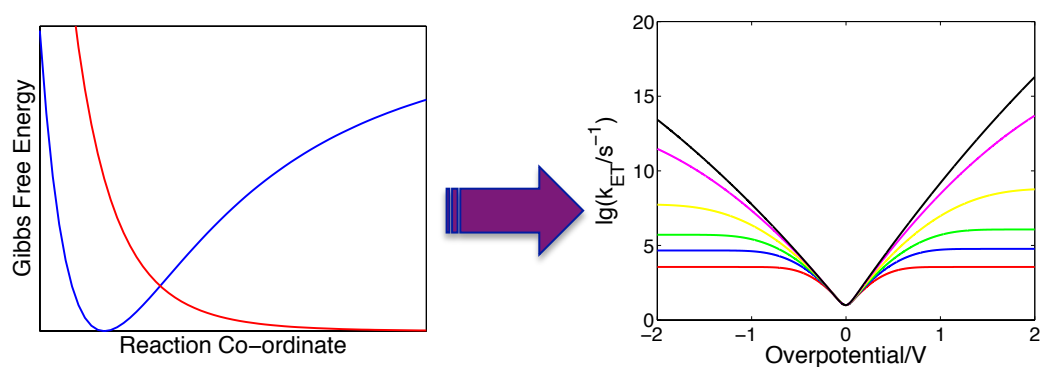
Anharmonicity, asymmetry, dissociation, electrochemistry, electron transfer, Marcus theory, self-assembled monolayer

### References

- [1] D. Pletcher, F. C. Walsh, *Industrial Electrochemistry*, 2<sup>nd</sup> edn., Kluwer, London, 1990.
- [2] M. C. Henstridge, E. Laborda, N. V. Rees, R. G. Compton, *Electrochim. Acta* **2021**, *84*, 12.
- [3] E. Laborda, M. C. Henstridge, C. Batchelor-McAuley, R. G. Compton, *Chem. Soc. Rev.* **2013**, *42*, 4894.
- [4] A. R. Despić, J. O'M. Bockris, *J. Chem. Phys.* **1960**, *32*, 389.
- [5] Y. I. Kharkats, J. Ulstrup, *J. Electroanal. Chem.* **1975**, *65*, 555.
- [6] J.-M. Savéant, *J. Am. Chem. Soc.* **1987**, *109*, 6788.
- [7] J.-M. Savéant, *J. Am. Chem. Soc.* **1992**, *114*, 10595.
- [8] A. M. Kuznetsov, J. Ulstrup, *Phys. Chem. Chem. Phys.* **1999**, *1*, 5587.
- [9] E. German, R. R. Dogonadze, *J. Res. Inst. Catal., Hokkaido Univ.* **1972**, *20*, 34.
- [10] N. Brüniche-Olsen, J. Ulstrup, *J. Chem. Soc., Faraday Trans. II* **1978**, *74*, 1690.
- [11] R. R. Dogonadze, A. M. Kuznetsov, J. Ulstrup, *J. Theor. Biol.* **1977**, *69*, 239.
- [12] N. C. Søndergaard, J. Ulstrup, J. Jortner, *Chem. Phys.* **1976**, *17*, 417.
- [13] J. Ulstrup, J. Jortner, *J. Chem. Phys.* **1975**, *63*, 4358.
- [14] R. Chang, C. S. Johnson, Jr., *J. Am. Chem. Soc.* **1966**, *88*, 2338.
- [15] N. Hirota, *J. Am. Chem. Soc.* **1968**, *90*, 3603.
- [16] A. M. Kuznetsov, I. G. Medvedev, J. Ulstrup, *Electrochem. Commun.* **2000**, *2*, 135.
- [17] P. Morse, *Phys. Rev.* **1929**, *34*, 57.
- [18] T.-C. Lim, *Z. Naturforsch.* **2003**, *53a*, 615.

- [19] G. Mie, *Annal. Physik.* **1903**, *11*, 657.
- [20] S. G. Christov, *J. Electroanal. Chem.* **1979**, *100*, 513.
- [21] A. M. Kuznetsov, J. Ulstrup, *Phys. Chem. Chem. Phys.* **1999**, *1*, 5587.
- [22] A. M. Kuznetsov, *J. Phys. Chem. A* **1999**, *103*, 1239.
- [23] J.-M. Savéant, *J. Phys. Chem. B* **2002**, *106*, 9387.
- [24] R. A. Marcus, *J. Chem. Soc., Faraday Trans.* **1996**, *92*, 3907.
- [25] W. Schmickler, *J. Electroanal. Chem.* 1979, *100*, 533.
- [26] A. A. Kornyshev, W. Schmickler, *J. Electroanal. Chem.* **1985**, *185*, 253.
- [27] W. Schmickler, *J. Electroanal. Chem.* 1986, *204*, 31.
- [28] W. Schmickler, *Chem. Phys. Lett.* **1995**, *237*, 152.
- [29] M. T. M. Koper, W. Schmickler, *Chem. Phys.* **1996**, *211*, 123.
- [30] F. London, M. Polanyi, *Naturwissenschaft.* **1930**, *18*, 1099.
- [31] H. C. Hamaker, *Physica* **1937**, *4*, 1058.
- [32] X. Wang, S. Ramírez-Hinestrosa, J. Dobnikar, D. Frenkel, *Phys. Chem. Chem. Phys.* **2020**, *22*, 10624.
- [25] J.-P. Hansen, I. R. McDonald, *Theory of Simple Liquids*, 2<sup>nd</sup> edn., Academic Press, London, 1986.
- [33] F. F. Abraham, Y. Singh, *J. Chem. Phys.* **1977**, *67*, 2384.
- [34] C. T. Lee, J. A. MacCammon, P. J. Rossky, *J. Chem. Phys.* **1984**, *80*, 4448.
- [35] L. N. Glosli, M. R. Philpott, *Electrochim. Acta* **1996**, *41*, 2145.
- [36] J.-M. Savéant, *J. Phys. Chem. B* **2001**, *105*, 8995.
- [37] J.-M. Savéant, *J. Phys. Chem. B* **2001**, *105*, 8995.
- [38] R. Nazmutdinov, P. Quaino, E. Colombo, E. Santos, W. Schmickler, *Phys. Chem. Chem. Phys.* **2020**, *22*, 13923.
- [39] (a) Y. S. Kim, R. G. Gordon, *J. Chem. Phys.* **1974**, *60*, 4332; (b) Y. Marcus, G. Hefter, *Chem. Rev.* **2006**, *106*, 4585; (c) S. Roy, M. D. Baer, C. J. Mundy, G. K. Schenter, *J. Chem. Theory Comput.* **2017**, *13*, 3470.
- [40] (a) S. Kumar, R. Nussinov, *Biophys. J.* **2002**, *83*, 1595; (b) J. R. Pliego, Jr., *Org. Biomol. Chem.* **2021**, *19*, 1900.
- [41] R. W. Gurney, *Proc. R. Soc. Lond. A* **1931**, *134*, 137.
- [42] H. Gerisher, *Z. Phys. Chem.* **1960**, *26*, 223.
- [43] R. R. Dogonadze, Y. A. Chizmadzhev, *Dolk. Akad. Nauk. SSSR* **1962**, *145*, 849.
- [44] R. R. Dogonadze, *Dolk. Akad. Nauk. SSSR* **1962**, *142*, 1108.
- [45] E. D. German, A. M. Kuznetsov, *Electrochim. Acta* **1981**, *26*, 1595.
- [46] P. Siders, R. A. Marcus, *J. Am. Chem. Soc.* **1981**, *103*, 741.
- [47] W. E. Wentworth, R. George, H. Keith, *J. Chem. Phys.* **1969**, *51*, 1791.
- [48] E. D. German, A. M. Kuznetsov, *J. Phys. Chem.* **1994**, *98*, 6120.
- [49] E. D. German, A. M. Kuznetsov, V. A. Tikhomirov, *J. Phys. Chem.* **1995**, *99*, 9095.
- [50] R. R. Dogonadze, A. M. Kuznetsov, *Prog. Surf. Sci.* **1975**, *6*, 1.
- [51] R. A. Marcus, *Can. J. Chem.* **1959**, *37*, 155.
- [52] K. S. Weber, S. E. Creager, *J. Electroanal. Chem.* **1998**, *458*, 17.
- [53] E. L. Yee, M. J. Weaver, *Inorg. Chem.* **1980**, *19*, 1077.
- [54] S. Sahami, M. J. Weaver, *J. Solution Chem.* **1981**, *10*, 199.
- [55] J. F. Smalley, S. W. Feldberg, C. E. D. Chidsey, M. R. Linford, M. D. Newton, Y.-P. Liu, *J. Phys. Chem.* **1995**, *99*, 13141.
- [56] G. K. Rowe, S. E. Creager, *Langmuir* **1991**, *7*, 2307.
- [57] S. E. Creager, G. K. Rowe, *J. Electroanal. Chem.* **1997**, *420*, 291.
- [58] K. Uosaki, Y. Sato, H. Kita, *Langmuir* **1991**, *7*, 1510.
- [59] F. Goujon, C. Bonal, B. Limoges, P. Malfreyt, *J. Phys. Chem. B* **2010**, *114*, 6447.
- [60] G. Filippini, F. Goujon, C. Bonal, P. Malfreyt, *Soft Mater.* **2011**, *7*, 8961.
- [61] D. B. Robinson, C. E. D. Chidsey, *J. Phys. Chem. B* **2002**, *106*, 10706.
- [62] E. J. F. Dickinson, R. G. Compton, *J. Electroanal. Chem.* **2011**, *661*, 198.
- [63] H. L. Tavernier, M. D. Fayer, *J. Phys. Chem. B* **2000**, *104*, 11541.
- [64] W. R. Fawcett, *Cond. Matter Phys.* **2005**, *8*, 413.
- [65] D. T. Boyle, X. Kong, A. Pei, P. E. Rudnicki, F. Shi, W. Huang, Z. Bao, J. Qin, Y. Cui, *ACS Energy Lett.* **2020**, *5*, 701.
- [66] S. Sripad, D. Korff, S. C. DeCaluwe, V. Viswanathan, *J. Chem. Phys.* **2020**, *153*, 194701.

## Graphical Abstract



A Lennard-Jones 9-3 interaction is used to explore the occurrence of asymmetric and anharmonic effects in electrochemical electron transfer processes. The features of the asymmetric Tafel plots are shown to capture the qualitative features of earlier models exploring anharmonic electron transfer at electrodes. Whilst weaknesses in the model are discussed, it is used to review electrochemical kinetics in ferrocene-based self-assembled monolayers bathed by perchloric acid: significant interactions between the ferricenium and perchlorate ions, suggestive of ion pairing, occur.